BUTTERWORTH HEINEMANN

Flow characteristics of an air-filled bayonet tube under laminar conditions

Harpal Minhas, G. S. H. Lock, and Maolin Wu*
Department of Mechanical Engineering, University of Alberta, Edmonton, AB, Canada

This paper provides the details of a combined experimental and numerical study of the bayonet tube under laminar conditions when the fluid is air. Attention is focused on the flow and frictional characteristics of the tube. The data constitute a systematic investigation of the effect of the principal parameters on the overall pressure drop, represented by an Euler number. Specifically discussed are the effects of Reynolds number, length–diameter ratio, the ratio of annular to inner tube area, and the ratio of the end clearance to the tube diameter. A complimentary series of visual studies is also described.

Keywords: bayonet tube; heat exchanger; laminar

Introduction

The bayonet tube consists of two concentric tubes, one end of the inner tube reaching close to the sealed end of the outer one. Thus, fluid flowing within and toward the open end of the inner tube is constrained to return along the annular gap formed between the two tubes. As a heat exchanger, the system has found extensive use in situations where the medium to be heated or cooled is either too large to be treated in its entirety or is readily accessible from one side only. The medium is then penetrated by the insertion of bayonet tubes, in contrast to the more common arrangement of tubes crossing back and forth. A more extensive discussion is given by Lock (1992).

The bayonet tube may be used in a geotechnical context to penetrate the Earth's surface. In regions containing sporadic permafrost, for example, the internal circulation of a refrigerant, or cold winter air, serves to maintain the ground in a frozen state in which it can support such engineering structures as towers, buildings, or roads (Jahns et al. 1973; Haynes and Zarling 1982). Similarly, bayonet tubes inserted through the winter ice cover on a river may be used to create a submerged wall of ice to facilitate the control of spring run-off (Lock 1986).

The use of bayonet tubes in the process industry was cited as early as 1946 (Hurd). The tubes, then called "field tubes," were used in vacuum condensers, suction tank heaters, and alkylation contactors. Recent industrial uses include: a potassium condenser boiler in a binary cycle power plant (Fraas 1973), a counterflow heat exchanger in a chemical processing plant (Zhang and Zhang 1988), a water tube reformed gas boiler in an ammonia plant (Hinchley 1984), and a high-temperature burner duct recuperator in a steel mill soaking pit (Luu and Grant 1985).

In previous work (Lock and Kirchner 1988; Lock and Kirchner 1990) it was noted that the flow in wind-driven thermosyphons was not only closely related to that in bayonet tubes, but would likely extend well into the laminar range. Accordingly, the present paper is devoted to a systematic study of frictional behavior in an air-filled bayonet tube under laminar conditions. Both experimental and numerical studies have been performed over a wide range of the governing parameters: Reynolds number, length–diameter ratio, diameter ratio, and end clearance ratio. Also, the main series of experiments were accompanied by visual flow experiments.

Experiments

Rig

A schematic representation of the rig is given in Figure 1. This consisted of a 2.57-cm diameter D copper tube with a length L varying from 25.7 cm to 102.8 cm; the overall length–diameter ratio (L/D), thus, ranged from 10 : 1 to 40 : 1. Inside this was inserted another tube made of acrylic. The inner diameter d_i of this inner tube was varied over the range $1.07\ \text{cm} < d_i < 1.99$ cm; its wall thickness also varied slightly (from 1.06 mm to 1.2 mm). The inner tube was aligned concentrically with the main tube and extended to a distance H (from the closed lower end) which was varied so that $0.034 < H/D < 2.05$.

The air entering the inner tube came directly from a settling chamber, which in turn, was supplied from the building mains. Prior to entering the settling chamber, however, the air was depressurized in a flow regulator positioned upstream of a control valve. Located well downstream of this valve was a laminar flow meter (Meriam Instruments 50 MJ 10). No attempt was made to control the air leaving the apparatus; it was allowed to discharge into quiescent room air. After leaving the settling chamber, the air entered the inner tube, traveling at least 50 diameters before emerging at the bottom.

The pressure difference across the flow meter was measured with a Validyne transducer (DP 15-30), the signal from which was read on a digital multimeter after demodulation. The mass flow rate thus determined was used to calculate mean velocities by invoking continuity; density was calculated from the local temperature and pressure using the ideal gas equation of state.

Address reprint requests to Professor Harpal Minhas, Department of Mechanical Engineering, University of Alberta, 4-9 Mechanical Engineering Building, Edmonton, AB T6G 2G8 Canada.

* Permanent address: University of Science and Technology, Beijing, People's Republic of China.

Received 30 August 1994; accepted 7 December 1994

Int. J. Heat and Fluid Flow 16: 186–193, 1995

655 Avenue of the Americas, New York, NY 10010

0142-727X/95/$10.00
SSDI 0142-727X(94)0020-D

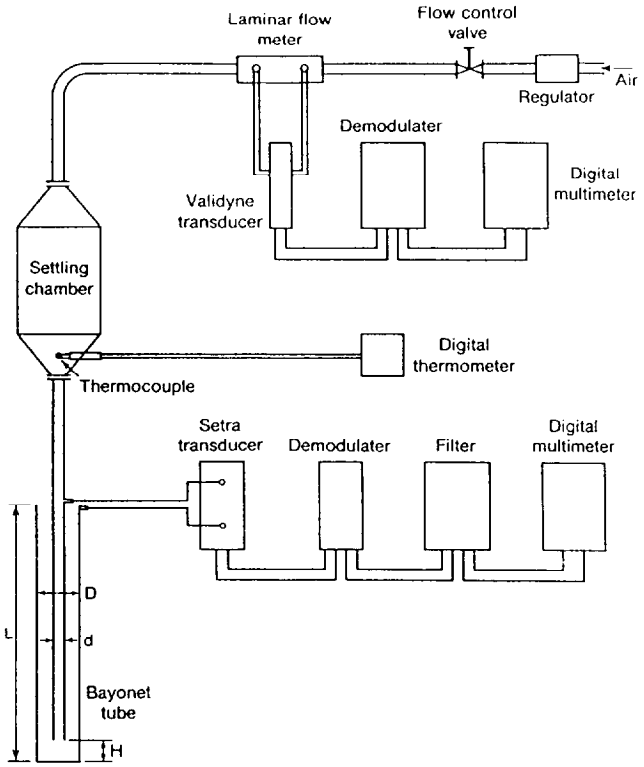

Figure 1 Schematic of apparatus

Static pressure was measured at two points having essentially the same elevation, both corresponding to the mouth of the bayonet tube. The pressure difference was measured with a Setra transducer; the signal was read on a digital multimeter following demodulation and filtering.

Experimental procedure

Before the bayonet tube experiments were begun, frictional loss in the inner tube was compared to the classical relationship $f = 64/\mathrm{Re}$ where $f = 2d\Delta P/\rho LU^2$ and the Reynolds number $\mathrm{Re} = Ud/\nu$ for steady, laminar, fully developed flow in a circular tube. With an upstream length much greater than $0.065d\mathrm{Re}$, the results obtained established that accuracy in pressure and flow rate were adequate for present purposes. Representative experimental errors obtained from a formal error analysis are discussed later.

With calibration completed, the experiments were conducted as follows. The flow control valve was opened carefully, and the system was allowed to reach equilibrium, as determined by the temperature of the air leaving the setting chamber. The flow pressure measuring systems were switched on and allowed to stabilize. Readings of temperature, flow rate, and pressure drop were then recorded. After altering the setting of the control valve, the procedure was repeated until a complete curve of pressure drop *versus* flow rate had been obtained for laminar conditions.

Definitions

Curves were thus obtained for various values of the governing parameters defined as follows.

(1) Length–diameter ratio: L/D, where L and D are length and diameter, respectively, of the outer tube.
(2) Area ratio: F_i/F_a, where

$$F_i = \frac{\pi}{4} d_i^2 \qquad \text{and} \qquad F_a = \frac{\pi}{4}(D^2 - d_o^2) \tag{1}$$

This replaces the simpler diameter ratio d/D by recognizing that d_i, the inside diameter of the inner tube, is not the same as its outside diameter d_o.
(3) Clearance ratio: H/D, where H is the end clearance of the inner tube.
(4) Reynolds number: For a single, circular tube, the definition given earlier will suffice, but the choice of a representative length is not so obvious for a concentric tube arrangement. In general, the Reynolds number may be defined in terms of the mass flow rate $\dot{m}$ by taking

$$\mathrm{Re} = \frac{\dot{m}}{\rho\nu}\left(\frac{Z}{A}\right) \tag{2}$$

Notation

A	area
d	inner tube diameter
D	outer tube diameter
Eu	Euler number
f	friction coefficient
F	area
H	end clearance
K	length–diameter ratio
l	inner tube length
L	outer tube length
m	mass
P, p	pressure
R, r	radial distance
Re	Reynolds number
U, u	axial velocity
V, v	radial velocity
W, w	circumferential velocity
X, x	axial distance

Greek

Θ, θ	circumferential distance
μ	fluid dynamic viscosity
ν	momentum diffusivity
ρ	mass density

Subscripts

a	annulus
c	characteristic
i	inner
o	outer
t	transducer

Superscript

•	per unit time

where Z and A are the appropriate length and cross-sectional area, respectively. For the annulus

$$\left(\frac{Z}{A}\right)_a = \frac{4}{\pi(D + d_o)} \tag{3}$$

whereas, for the inner tube

$$\left(\frac{Z}{A}\right)_i = \frac{4}{\pi d_i} \tag{4}$$

Hence by defining

$$\mathrm{Re}' = \frac{4\dot{m}D}{\rho\pi\nu(D + d_o)d_i} = \mathrm{Re}_a \frac{D}{d_i} \tag{5}$$

the appropriate limiting forms when $d_i \ll D$ or $d_i \approx D$ may be recovered provided that $(d_o - d_i)/D \ll 1$. Equation 5 thus provides a simple and convenient definition that covers the full range of F_i/F_a.

(5) Euler number: A similar problem exists in non-dimensionalizing the pressure drop that incorporates two main effects: viscous and inertial. The structure given in Equation 5 is equivalent to taking the characteristic "diameter" as

$$D_c = \frac{d_i(D - d_o)}{D} \tag{6}$$

and the characteristic velocity as

$$U_c = \frac{4\dot{m}D^2}{\rho\pi(D^2 - d_o^2)d_i^2} = U_a\left(\frac{D}{d_i}\right)^2 \tag{7}$$

This permits an Euler number to be defined by

$$\mathrm{Eu} = \frac{2\Delta P}{\rho(U_c)^2} \tag{8}$$

where, using the energy equation between inlet and outlet,

$$\Delta P = \Delta P_t + \rho U_i^2\left[1 - \frac{3}{4}\left(\frac{F_i}{F_a}\right)^2\right] \tag{9}$$

in which ΔP_t is the pressure drop across the transducer, and the known velocity profiles for fully developed flow in a tube and annulus have been incorporated.

Flow visualization

Visual studies were also undertaken with the outer (metal) tube replaced by a plexiglass tube of the same fixed diameter (25.72 mm). Inside the plexiglass tube, an adjustable piston enabled variations in the end clearance of the inner tube to be made. Smoke injected into the air supply provided details of the flow pattern in the end region. Photographs of the streamlines thus generated were obtained with a light slit that illuminated a plane containing the axis and a diameter of the tube.

Numerical analysis

Governing equations and boundary conditions

Flow in a bayonet tube is governed by the continuity and momentum equations, here expressed in cylindrical coordinates. The following dimensionless parameters were introduced:

Displacement:

$$x = \frac{X}{L}, \quad r = \frac{\mathrm{R}}{\mathrm{R}_o}, \quad \theta = \frac{\theta}{2\pi} \tag{10}$$

Velocity:

$$u = \frac{U}{\left(\frac{4K\nu}{D}\right)}, \quad v = \frac{V}{\left(\frac{4K\nu\mathrm{R}_o}{DL}\right)}, \quad w = \frac{W}{\left(\frac{8\pi K\nu\mathrm{R}_o}{DL}\right)} \tag{11}$$

Pressure:

$$p = \frac{P - P_L}{\left(\frac{16\rho K^2\nu^2}{D^2}\right)} \tag{12}$$

where $K = L/D$ and P_L is the reference pressure at the entry.

For a steady, laminar flow of a Newtonian, Boussinesquian fluid, the nondimensionalized governing equations may be written as:

$$\frac{\partial u}{\partial x} + \frac{1}{r}\frac{\partial}{\partial r}(rv) + \frac{1}{r}\frac{\partial w}{\partial \theta} = 0 \tag{13}$$

$$u\frac{\partial u}{\partial x} + v\frac{\partial u}{\partial r} + \frac{w}{r}\frac{\partial u}{\partial \theta} = -\frac{\partial p}{\partial x} + \frac{1}{\mathrm{Re}\,K}\frac{\partial^2 u}{\partial x^2} + \frac{4K}{\mathrm{Re}}\frac{1}{r}\frac{\partial}{\partial r}\left(r\frac{\partial u}{\partial r}\right) + \frac{K}{\pi^2\mathrm{Re}}\frac{1}{r^2}\frac{\partial^2 u}{\partial \theta^2} \tag{14}$$

$$u\frac{\partial v}{\partial x} + v\frac{\partial v}{\partial r} + \frac{w}{r}\frac{\partial v}{\partial \theta} = -4K^2\frac{\partial p}{\partial r} + \frac{1}{\mathrm{Re}\,K}\frac{\partial^2 v}{\partial x^2} + \frac{4K}{\mathrm{Re}}\frac{1}{r}\frac{\partial}{\partial r}\left(r\frac{\partial v}{\partial r}\right) + \frac{K}{\pi^2\mathrm{Re}}\frac{1}{r^2}\frac{\partial^2 v}{\partial \theta^2} - \frac{4K}{\mathrm{Re}}\frac{v}{r^2} - \frac{8K}{\mathrm{Re}}\frac{1}{r^2}\frac{\partial w}{\partial \theta} + 4\pi^2\frac{w^2}{r} \tag{15}$$

$$u\frac{\partial w}{\partial x} + v\frac{\partial w}{\partial r} + \frac{w}{r}\frac{\partial w}{\partial \theta} = -\frac{K^2}{\pi^2}\left(\frac{1}{r}\frac{\partial p}{\partial \theta}\right) + \frac{1}{\mathrm{Re}\,K}\frac{\partial^2 w}{\partial x^2} + \frac{4K}{\mathrm{Re}}\frac{1}{r}\frac{\partial}{\partial r}\left(r\frac{\partial w}{\partial r}\right) + \frac{K}{\pi^2\mathrm{Re}}\frac{1}{r^2}\frac{\partial w}{\partial \theta^2} - \frac{4K}{\mathrm{Re}}\frac{w}{r^2} + \frac{2K}{\pi^2\mathrm{Re}}\frac{1}{r^2}\frac{\partial v}{\partial \theta} - \left(\frac{vw}{r}\right) \tag{16}$$

where

$$\mathrm{Re} = \frac{\left(\frac{4K\nu}{D}\right)D}{\nu} = 4K \tag{17}$$

because

$$u_c = \frac{4K\nu}{D} \tag{18}$$

The tube diameter ratio D/d does not appear explicitly above; it is incorporated implicitly through the equations given in the *Definition* section.

A parabolic velocity profile was assumed at the tube entrance. Velocity at all walls was taken to be zero. Symmetry and periodicity were assumed at the tube center and periodicity

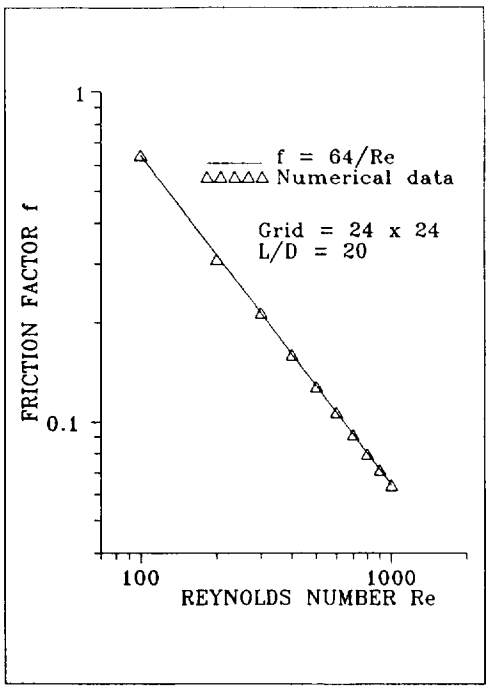

Figure 2 Comparison of friction factor data for fully developed laminar flow in a circular tube

plane ($\Theta = 0, 2\pi$), respectively. At the tube exit, a Neumann boundary condition (zero axial gradient) was set for velocity.

Algorithm and program validation

The numerical simulation was done using the algorithm of Patankar (1980) in the SIMPLE-C version suggested by Van Doormaal and Raithby (1984). The program was validated for steady, laminar, constant property, axisymmetric, air flow in a straight pipe with no inner tube. A fully developed velocity profile was assumed at the inlet and a length–diameter ratio of 20 was used. The latter was chosen as a representative "standard" value for which the bayonet tube is studied later. An optimum relaxation factor of 0.72 was used. The convergence criterion required agreement of successive averaged values of the dependent variables to be within 1%—agreement was usually better than this. As expected, the percentage mass error between the inlet and outlet decreased with grid size. Based on a comparative study of different grid sizes, a 24 × 24 grid was chosen. The percentage mass error between the inlet and outlet for this grid was less than 0.6%.

Accuracy was checked using a friction factor—Reynolds number plot. The results are compared with the classical relation $f = 64/\mathrm{Re}$ in Figure 2; good agreement is evident, revealing an accuracy of $\pm 1\%$.

For the complete bayonet tube, the same convergence criterion was used. However, a 41 × 41 × 20 grid was then used because two pipes were being considered. It was anticipated that a finer grid would be needed to accommodate a more complex flow field. An optimum relaxation factor of 0.72 was used again. The program was first run at "standard" parametric values: $\mathrm{Re}' = 1000$, $L/D = 20$, $F_i/F_a = 0.474$ and $H/D = 1$ represent practical operational values for a bayonet tube. A test with a grid of 61 × 61 × 40 indicated an Euler number change of less than 2%, while the time taken to run the program was increased by more than 10%. The percentage mass error between the inlet and outlet was still less than 0.6%.

The results were spot checked for uniqueness by using different initial fields. The solutions remained unchanged.

Results and discussion

The data discussed below all deal with the effect of the controlling parameters on the Euler number as defined by Equation 8. During each parametric exploration, the other parameters were held constant at the same set of "reference" values given above. Discrete numerical points have been converted into curves using a cubic spline.

Effect of Reynolds number

The effect of the Reynolds number on the Euler number is shown in Figure 3. As expected, the Euler number decreases monotonically with an increase in the Reynolds number, here plotted on a logarithmic scale. This trend is not unexpected given the shape of the curve in Figure 3. In view of the abrupt change of direction, it is unlikely the flow would remain laminar up to a Reynolds number of 2500; we arbitrarily truncated the results at $\mathrm{Re}' = 1000$.

The numerical prediction is seen to lie consistently below the experimental data, percentage deviations being larger at Reynolds numbers near the two extremes of the curve: experimental points (1) and (4) are above the numerical curve by 23.5% and 12.3%, respectively. Experimental point (1) is plotted for $F_i/F_a = 0.229$; as will be seen later, the Euler number for an area ratio of 0.229 is about 20% more than that at 0.474 (see the *Effect of area ratio* section). Also, experimental point (4) is for a clearance ratio of 0.748; the Euler number for $H/D = 0.748$ is about 12.5% than for $H/D = 1.0$ (see the *Effect of clearance ratio* section). Agreement at these points is, thus, within the experimental error of 10%. The discrepancy at points (2) and (3) is more difficult to explain, but is not very great (13.6 and 21.6%, respectively).

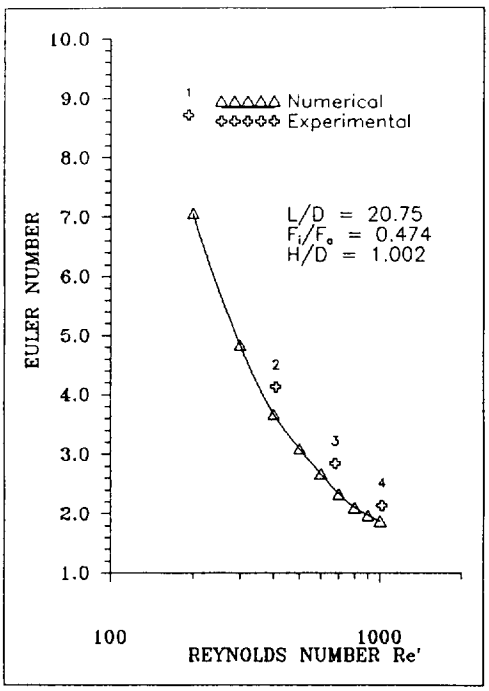

Figure 3 Effect of Reynolds number on Euler number

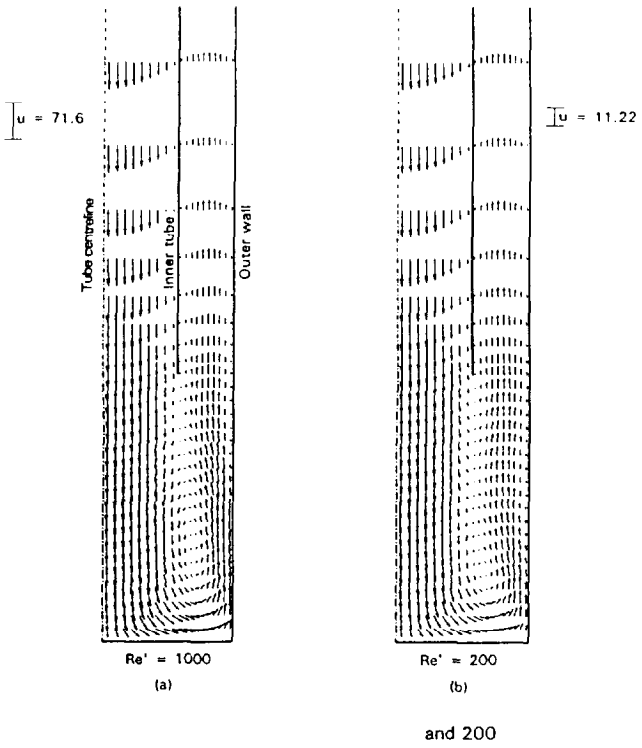

Figure 4 Velocity fields for Re' = 1000 and 200

The flow patterns for the widely separated Reynolds numbers of 200 and 1000 were studied, the respective velocity fields being shown in Figure 4, the left side of which provides the "standard" flow field for future comparison. A ring vortex is observed in the end clearance zone. This vortex had a stable, axisymmetric form. As the fluid moves away from the sealed end, the vortex is pinched slightly. At Re' = 200, it splits into several small secondary, and very weak, vortices before reattaching at the outside of the inner tube. At Re' = 1000, the velocities are higher, and the circulation within the vortex is correspondingly greater. A stronger vortex implies a greater dissipation rate, which in turn, implies a greater pressure drop.

Effect of length–diameter ratio

The effect of length–diameter ratio L/D on Euler number is shown in Figure 5. As expected, the Euler number increases with an increase in the length–diameter ratio. This linear trend is expected to continue for L/D values greater than 40, because the skin friction loss increases in proportion to the tube surface area.

At $L/D = 30$, corresponding to experimental point (3), the numerical results are within $\pm 10\%$ experimental data. For other points, the deviation is caused by variations in the experimental parameters. Point (1), for example, is for a Reynolds number of 689. As seen in the previous section, a decrease in the mass flow rate results in an increase in pressure drop. Hence, point (1) should lie about 27% above the numerical data; it is slightly higher (42.5%) for reasons unknown. Point (2) is for $H/D = 0.748$ implying that it should lie about 12.6% above the numerical curve; it is 14.6% above. Also point (4), which is about 12% above the numerical curve, should be 2% greater, because it is for a clearance ratio of 0.982 (see the *Effect of clearance ratio* section). Agreement for points (2), (3), and (4) is, therefore, within experimental error of 10%. The neglect of the inner tube thickness in the numerical study appears to create a small systematic error.

Effect of area ratio

The effect of the area ratio, F_i/F_a, on the Euler number, is illustrated in Figure 6. The variation of the Euler number with the area ratio is clearly complex. Appearance of the minimum might have been expected at $F_i/F_a = 1.0$, when the inertial contribution to the pressure drop is theoretically zero; i.e., when sudden contraction or expansion does not occur. However, this prescription of inertial behavior does not account for the space created by the end clearance or the refluent flow in the end zone. It is evident from the figure that the pressure drop is controlled by the smaller of F_i and F_a. Deviations from experimental data may again be explained by the differences in parametric values.

It was observed from the velocity field for $F_i/F_a = 0.2$ that the ring vortex again formed in the clearance space, but was then accompanied by a weak secondary vortex on the outer tube. At even lower area ratios, the flow within this secondary vortex became more vigorous and thus presented more resistance. For area ratios above 0.2, the secondary vortex diminished until at $F_i/F_a \approx 0.47$ (see Figure 4a), it vanishes completely resulting in a minimum, with a single ring vortex in the clearance space. For area ratios greater than this pessimal value, fluid begins to move in the circumferential direction. A three-dimensional (3-D) flow thus emerges, beginning near the sealed end and gradually spreading as the area ratio increases.

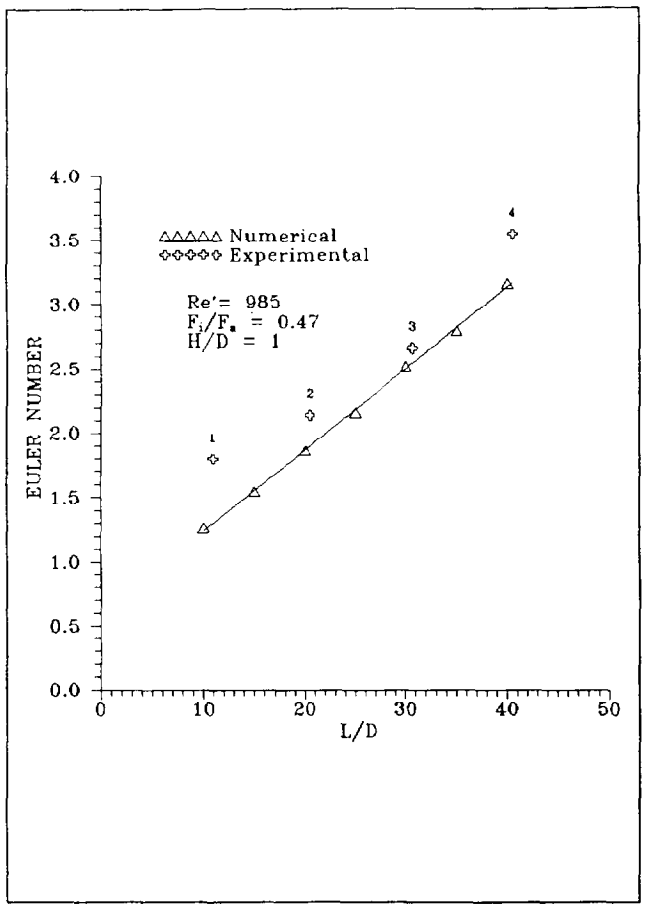

Figure 5 Effect of length–diameter ratio on Euler number

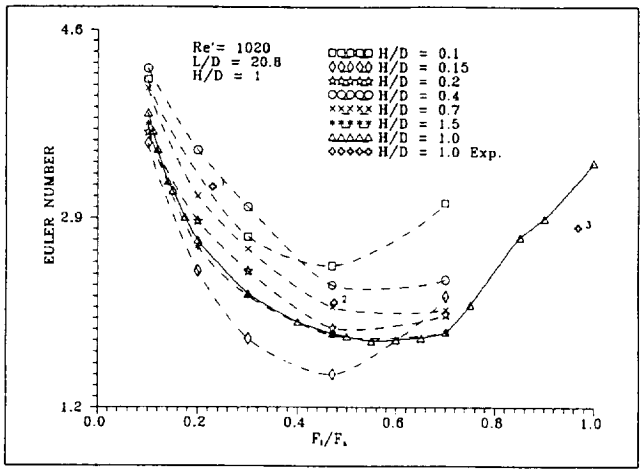

Figure 6 Effect of area ratio on Euler number

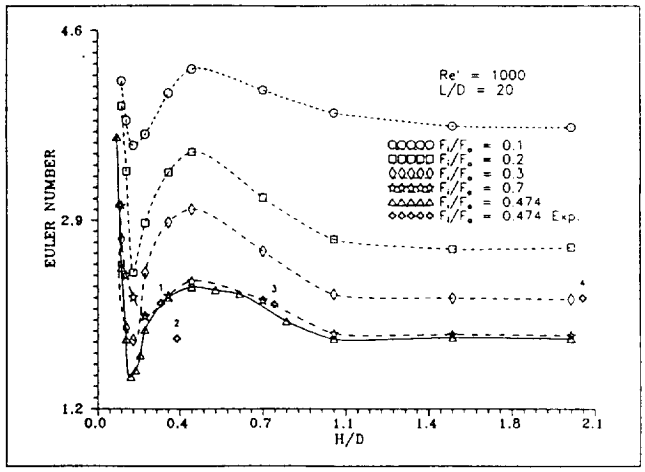

Figure 7 Effect of clearance ratio on Euler number

For an area ratio of 1.5, the 3-D effects were considerable near the bottom. At midheight in the clearance zone, these effects vanish, and the flow became axisymmetric. However, they evolve again near the end of the inner tube, being more dominant in the annular space and near the inside wall of the inner tube. This suggests that the decreased exit area is responsible for their origin. They gradually die out as the fluid advances upward along the annulus. At even higher ratios, it is to be expected that the 3-D effects would extend to the mouth of the annulus. In practical terms, however, the higher values of Eu produced when $F_i/F_a \geq 0.7$ tend to be of academic interest.

Effect of clearance ratio

The effect of clearance ratio is shown in Figure 7. This is, in essence, a cross plot of Figure 6 and clearly reveals a family of curves. A comparison with sparse experimental data again indicates that deviations are attributable to differences in parametric values. For very small clearances, that is $H/D < 0.1$, the effect of reducing H/D is to produce a high pressure gradient. This is attributable to two factors: the reduced clearance space and a flow separation phenomenon, as explained later. For $H/D > 1$, the pressure drop is nearly constant, as expected. For $0.1 < H/D < 1$, two extrema are observed, a minimum and a maximum, which occur at $H/D \approx 0.15$ and 0.4, respectively.

Velocity fields for $H/D = 0.15$ revealed a ring of separation on the outside of inner tube. A small secondary vortex circulating in the opposite direction was also observed in the bottom corner. For clearance ratios less than the minimum, corresponding to $H/D = 0.15$ in the figure, the secondary corner vortex became enlarged with further decreases in clearance ratio. This, along with the ring of separation evidently accounts for a higher pressure drop for very small values of H/D. At $H/D = 0.15$, the secondary corner vortex virtually disappeared, thus accounting for the minimum. For clearance ratios increasing between 0.15 and 0.4, the ring of separation grew further, accounting for greater pressure drops. For H/D values between 0.4 and 1.0, the ring occupied less and less of the inner tube wall, eventually becoming a full-fledged vortex, thus decreasing the pressure drop. For $H/D = 1.0$ (the reference condition; see Figure 4a), a full-fledged vortex is observed at the mouth of the inner tube.

Streamlines from the numerical study are compared with those obtained by visualization in Figures 8 and 9. Despite the slight differences in scale, the flow patterns are seen to be very similar.

Empirical correlation

The selected results given above are a systematic attempt to uncover the effect of geometry and flow rate on hydraulic behavior. However, although they provide a useful sensitivity study, they are limited in their direct and immediate application to a wide range of industrial and geotechnical situations. To circumvent this restriction, the entire set of experimental data obtained was used to develop a empirical correlation with Euler number (and, hence, the pressure drop) as the dependent variable. The results are shown in Figure 10.

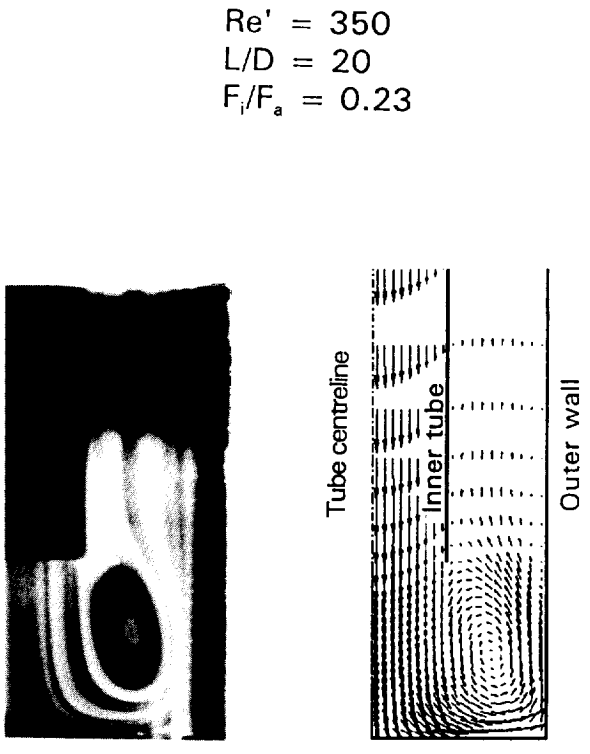

Figure 8 Velocity field for $H/D = 0.5$

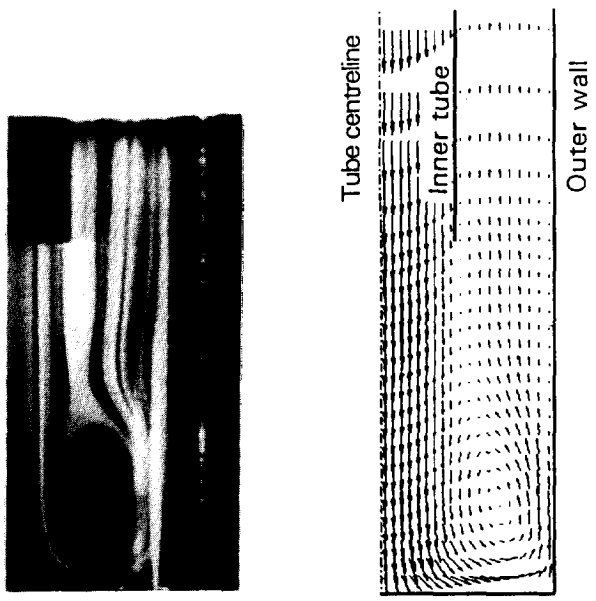

Figure 9 Velocity field for $H/D = 1.0$

To construct a suitable empirical correlation form, it was decided at the outset that the effect of Reynolds number could be accurately represented by a power law, as suggested by Figure 4. A similar assumption was also made for the effect of length–diameter ratio. The simple power law relation does not, however, describe the effect of area ratio and clearance ratio, as Figures 6 and 7 reveal. For the former, an attempt was made to approximate the minimum seen in Figure 6 by taking a simple parabolic form. By trial and error, the functions best reflecting the clearance ratio data were found to be power law products. The general relationship was thus constructed in the following form:

$$\mathrm{Eu} = A_0\left(\frac{L}{D}\right)^{\alpha} \frac{f(H/D, F_i/F_a)}{\mathrm{Re}^{\beta}} \tag{19}$$

where α and β are exponents and

$$f = \left[a + \left(\frac{f_i}{F_a} - b\right)^2\right]^{c}\left[c + \left(\frac{H}{D} - e\right)^2\right]^{g}\left[\frac{H}{D}\left(\frac{F_i}{F_a}\right)^{1/2}\right]^{\varepsilon} \tag{20}$$

This empirical equation resulted in

$$\mathrm{Eu} = 110G \tag{21}$$

where

$$G = \frac{(L/D)^{0.75}}{\mathrm{Re}^{0.81}}\left[8 \times 10^{-4} + \left(\frac{F_i}{F_a} - 0.64\right)^2\right]^{0.18}\left(\frac{D}{H}\right)^{0.31} \times \left[\frac{H}{D}\left(\frac{F_i}{F_a}\right)^{1/2}\right]^{0.28} \tag{22}$$

Figure 10 shows Equation 21 superimposed on the experimental and selected numerical data. With the exception of a few points, the data almost all fall within a band of $\pm 10\%$. This uncertainty is greater than the intrinsic measurement uncertainty of $\pm 5\%$, mainly because of the approximations made in the assumed empirical form. It is, however, acceptable for many applications of the bayonet tube.

Conclusions

The paper presents the results of a combined experimental and numerical studies of the frictional characteristics of an air-filled bayonet tube under steady, laminar conditions. Good agreement was obtained between the numerical data, the experimental data and flow visualizations.

The results have been presented in terms of an Euler number Eu and Reynolds number Re' both of which have been defined to accommodate a wide range of tube geometries. The effect of Reynolds number was found to be as expected, with Eu decreasing following increases in Re'. Likewise, the observed increase in Eu with L/D was not unexpected.

The effect of diameter ratio or area ratio F_i/F_a was not found to be monotonic. Although the appearance of a minimum in Eu is consistent with the requirement that either the annulus or the inner tube will dominate frictional behavior when F_i/F_a is markedly different from unity, the location of the minimum uncovered the importance of the flow pattern in the end zone. An examination of the flow pattern under representative conditions revealed a ring vortex in the clearance zone, thus accounting for a low pressure drop. For area ratios less than

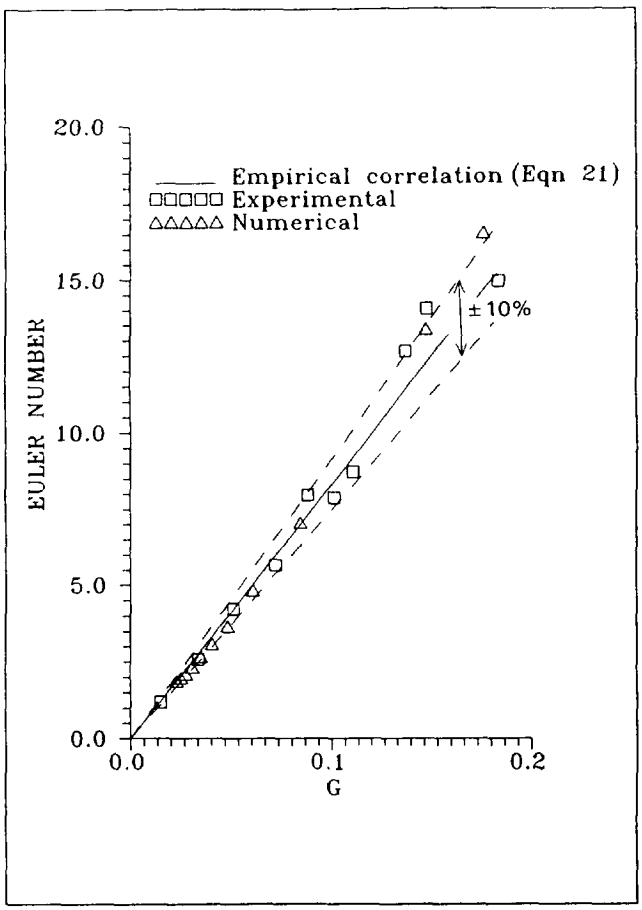

Figure 10 The empirical correlation

the minimum the existence of a secondary vortex along with the primary vortex accounted for higher pressure drops. For F_i/F_a values greater than the minimum, 3-D effects were the cause of higher frictional losses.

Very low values of the clearance ratio created a secondary corner vortex accounting for higher pressure drops. A diminishing secondary vortex along with a ring of separation corresponded to the minimum in the curve; a ring of separation alone corresponded to the maximum. A high value of Eu yielded a stable ring vortex.

The effects of individual parameters were converted in an empirical correlation. The correlation successfully described hydraulic behavior over a wide range of conditions, especially in the preferred design zone, where pressure loss is minimized.

Acknowledgments

This work was made possible by the Natural Sciences and Engineering Council of Canada and the government of China, to both of whom we are indebted. We also wish to thank K. C. Cheng for the use of equipment, and we acknowledge the invaluable assistance of the machinists and technicians of the Department of Mechanical Engineering, University of Alberta, particularly Alan Muir and Brian Cielin.

References

Fraas, A. P. 1973. A potassium–steam binary vapour cycle for better fuel economy and reduced thermal pollution. *J. Eng. Power*, **95**, 53–63

Haynes, F. D. and Zarling, J. P. 1982. A comparative study of thermosyphons used in freezing soil. ASME paper 82-Wa/HT- 40

Hinchley, P. 1984. Key aspects of the design and specification of individual items of plant. In *Heat Exchanger Design Handbook*, Vol. 3, B. A. Bolding and M. Prescott (eds.), Hemisphere, Washington, DC, 1–15

Hurd, N. L. 1946. Mean temperature difference in field or bayonet tube. *Ind. Eng. Chem.*, **38**, 1266–1271

Jahns, H. O., Miller, T. W., Power, L. D., Rickey, W. P., Taylor, T. P. and Wheeler, J. A. 1973. Permafrost protection for pipelines on permafrost. *2nd Int. Conf. on Permafrost*, National Academy Press, Washington, DC, 673–684

Lock, G. S. H. 1986. Control of spring run-off in northern rivers: The ice veil concept. *Polar Record*, 451–457

Lock, G. S. H. 1992. *The Tubular Thermosyphon*. Oxford University Press, Oxford, UK

Lock, G. S. H. and Kirchner, J. D. 1988. Performance of an air-filled, open thermosyphon tube with particular reference to wind augmentation. *Int. J. Heat Mass Transfer*, **31**, 2357–2364

Lock, G. S. H. and Kirchner, J. D. 1990. Wind augmentated heat transfer in an open thermosyphon tube with large length–diameter ratios. *J. Heat Transfer*, **112**, 71–77

Luu, M. and Grant, K. W. 1985. Thermal and fluid design of a bayonet tube heat exchanger for high-temperature waste heat recovery. In *Industrial Heat Exchangers*, A. J. Hayes, W. W. Wang, S. C. Richlen and E. S. Tabb (eds.), 159–173

Patankar, S. V. 1980. *Numerical Heat Transfer and Fluid Flow*. Hemisphere, Washington, DC

Van Doormaal, J. P. and Raithby, G. D. 1984. Enhancement of the SIMPLE method for predicting incompressible fluid flows. *Num. Heat Transfer*, **7**, 147–163

Zhang, Y. M. and Zhang, H. Q. 1988. Experimental investigation of flow characteristics about tip heat transfer in bayonet tube (in Chinese). *Huagong Jixie*, **15**, 96–102